Published in final edited form as:
J Am Chem Soc. 2008 July 30; 130(30): 9878–9886. doi:10.1021/ja802111w.

Stabilization of Fully Reduced Iron–Sulfur Clusters by Carbene Ligation: The $[Fe_nS_n]^0$ Oxidation Levels (n = 4, 8)

Liang Deng and **R. H. Holm**
Department of Chemistry and Chemical Biology, Harvard University, Cambridge, Massachusetts 02138, E-mail: holm@chemistry.harvard.edu

Abstract

The all-ferrous $[Fe_4S_4]^0$ state has been demonstrated in the fully reduced Fe protein of the *Azotobacter vinelandii* nitrogenase complex. We seek synthetic analogues of this state more tractable than the recently prepared but highly unstable cluster $[Fe_4S_4(CN)_4]^{4-}$ (Scott, Berlinguette, Holm, and Zhou, *Proc. Natl. Acad. Sci. U.S.A.* **2005**, *102*, 9741). The *N*-heterocyclic carbene 1,3-diisopropyl-4,5-dimethylimidazol-2-ylidene ($Pr^i_2NHCMe_2$) has been found to stabilize the fully reduced clusters $[Fe_8S_8(Pr^i_2NHCMe_2)_6]$ (**4**) and $[Fe_4S_4(Pr^i_2NHCMe_2)_4]$ (**5**), which are prepared by cluster assembly or phosphine substitution of Fe_nS_n (n = 8, 16) clusters. Cluster **4** is also obtained by reaction of the carbene with all-ferrous $[Fe_7S_6(PEt_3)_5Cl_2]$ (**3**) and cluster **5** by carbene cleavage of **4**. Detailed structures of **3** (monocapped prismatic), **4**, and **5** are described; the latter two are the first iron–sulfur clusters with Fe–Cσ bonds. Cluster **4** possesses the $[Fe_8(\mu_3\text{-}S)_6(\mu_4\text{-}S)_2]$ edge-bridged double cubane structure and **5** the cubane-type $[Fe_4(\mu_3\text{-}S)_4]$ stereochemistry. The all-ferrous formulations of the clusters are confirmed by X-ray structure parameters and ^{57}Fe isomer shifts. Both clusters are stable under conventional aprotic anaerobic conditions, enabling further study of reactivity. The collective properties of **5** indicate that it is a meaningful synthetic analogue of the core of the fully reduced protein-bound cluster.

Introduction

Cubane-type $Fe_4(\mu_3\text{-}S)_4$ clusters are ubiquitous cofactors of iron–sulfur proteins, many of which manifest electron transfer as their primary or only function.[1–3] These clusters are usually found in the fully cysteinate-ligated form $[Fe_4S_4(S_{Cys})_4]$ and commonly exhibit one of two redox couples: the $[Fe_4S_4]^{2+/3+}$ couple in high-potential proteins (+0.1 to +0.4 V) and the more frequently encountered $[Fe_4S_4]^{1+/2+}$ couple in low potential proteins (−0.3 to −0.7 V). The indicated potential ranges are approximate; individual cluster potentials are modulated by protein environmental factors such as orientation of proximate peptide dipoles, hydrogen bonding, and solvation and by noncysteinate ligation. The cluster cores are electronically delocalized; formal oxidation states associated with the core charges are specified in series 1.

$[Fe_4S_4]^0$	$[Fe_4S_4]^{1+}$	$[Fe_4S_4]^{2+}$	$[Fe_4S_4]^{3+}$
$4Fe^{2+}$	$3Fe^{2+}+Fe^{3+}$	$2Fe^{2+}+2Fe^{3+}$	$Fe^{2+}+3Fe^{3+}$

(1)

The Fe protein of nitrogenase has long been considered to utilize the $[Fe_4S_4]^{1+/2+}$ couple in transmitting electrons to the MoFe protein for substrate reduction.[4] However, the proposal in 1994 of a $[Fe_4S_4]^0$ state in the Fe protein[5] challenged the one-electron delivery concept and,

Correspondence to: R. H. Holm.

Supporting Information Available: X-ray structural data for the three compounds in Table 1. This material is available free of charge via the Internet at http://pubs.acs.org.

more generally, the existence of only three cluster oxidation states in proteins. Thereafter, extensive evidence has been assembled that demonstrates this state in the *Azotobacter vinelandii* Fe protein when reduced with two equiv of Ti^{III}(citrate).[6–10] In particular, the ^{57}Fe isomer shift of 0.68 mm/s (4.2 K)[9] proves the all-ferrous formulation and protein crystallography establishes retention of the cubane-type geometry with dimensional changes consistent with reduction of the $[Fe_4S_4]^{2+}$ state of the as-isolated protein.[10] The all-ferrous state is reached at the potential $E^{0/1+} \approx -0.79$ V vs NHE.[11,12] There is now unequivocal evidence for the existence of *four* oxidation states among protein-bound Fe_4S_4 clusters.

The possible function of the $[Fe_4S_4]^0$ state as a two-electron reductant in the reactions of nitrogenase[13–15] and the claim of a $S = 0$ ground state[16] in addition to the documented $S = 4$ state[9] are among the factors that create an imperative for the isolation and investigation of an all-ferrous cluster. We briefly summarize work directed toward that end. Synthetic analogue clusters $[Fe_4S_4(SR)_4]^{3-,2-,1-}$ have been isolated and extensively studied for all but the $[Fe_4S_4]^0$ oxidation level in series 1.[17]

The all-ferrous oxidation state was first detected in electro-chemical investigations of the analogue clusters $[Fe_4S_4(SR)_4]^{2-}$. Dependent on the substituent R, a small number of such clusters can be reversibly oxidized to $[Fe_4S_4(SR)_4]^{1-}$, but nearly all are reduced reversibly to $[Fe_4S_4(SR)_4]^{3-}$. Certain of these clusters can be further reduced reversibly or quasireversibly to $[Fe_4S_4(SR)_4]^{4-}$,[18] thereby providing evidence for the $[Fe_4S_4]^0$ state early in the development of analogue chemistry[19–21] and thereafter.[18] Because these clusters are formed at potentials $E_{1/2}^{4-/3-} \leq -1.6$ V vs SCE in acetonitrile or DMF,[18] they are highly sensitive to oxidizing impurities. Despite multiple attempts in this laboratory, no pure fully reduced thiolate cluster has ever been isolated. Reduction of preisolated phosphine clusters $[Fe_4S_4(PR_3)_4]^{1+}$ proceeds at less negative potentials ($E_{1/2}^{0/1+} \approx -(0.8$ to $1.0)$ V, R = alkyl); however, workup of chemically reduced products yielded all-ferrous products but as the double cubane $[Fe_8S_8(PR_3)_6]$ or the tetracubane $[Fe_{16}S_{16}(PR_3)_8]$.[22,23] Most recently, chemical reduction of the cyanide cluster $[Fe_4S_4(CN)_4]^{3-}$ ($E_{1/2}^{4-/3-} = -1.42$ V, dichloromethane) has led to the first isolation in substance of the elusive $[Fe_4S_4]^0$ state in the form of red crystalline $(Bu_4N)_4[Fe_4S_4(CN)_4]$.[24] However, the cluster is so sensitive that it cannot be recrystallized or sustained in solution without excess reductant present; otherwise very rapid oxidation or other decomposition ensues. We seek an all-ferrous cluster whose stability permits determination of physicochemical properties and investigation of reactivity on pure samples. We report here the synthesis and certain properties of a cluster type that is amenable to these purposes.

Experimental Section

Preparation of Compounds

All reactions and manipulations were performed under a pure dinitrogen using either Schlenk techniques or an inert atmosphere box. Solvents were passed through an Innovative Technology solvent purification system prior to use. Solvent removal steps were performed in vacuo.

$[Fe_7S_6(PEt_3)_5Cl_2]$

To a solution of $[FeCl_2(PEt_3)_2]$[25] (0.72 g, 2.0 mmol) in THF (10 mL) was added a solution of $(Me_3Si)_2S$ (0.54 g, 3.0 mmol) in THF (10 mL). The mixture was stirred overnight. Solvent was removed, the black oily residue was dissolved in THF (5 mL), and the solution was filtered. Vapor diffusion of *n*-hexane into the black filtrate affords the product as a black crystalline solid (0.26 g, 70%). It is freely soluble in benzene but slowly decomposes over several hours at room temperature. The compound was identified by an X-ray structure determination.

[$Fe_8S_8(Pr^i{}_2NHCMe_2)_6$]

Method A—To a solution of [$Fe_7S_6(PEt_3)_5Cl_2$] (0.25 g, 0.20 mmol) in benzene (10 mL) was added a solution of 1,3-diisopropyl-4,5-dimethylimidazol-2-ylidene[26] ($Pr^i{}_2NHCMe_2$, 0.18 g, 1.0 mmol) in benzene (5 mL). The reaction mixture was stirred for 4 h and filtered. Vapor diffusion of *n*-hexane into the brown filtrate caused separation of the product as a black crystalline solid (0.16 g, 52%). ^{1}H NMR (C_6D_6): δ 7.12 (2), 5.16 (2), 3.71 (2), 2.09 (1), 0.41 (2), −2.34 (br); (THF-d_8): 7.61 (2), 5.24 (2), 3.26 (2), 2.38 (1), 0.30 (2), −2.90 (br).

Method B—To a solution of [$FeCl_2(PPr^i{}_3)_2$] (0.45 g, 1.0 mmol; prepared by the method for [$FeCl_2(PEt_3)_2$]) in THF (10 mL) was added $(Me_3Si)_2S$ (0.36 g, 2.0 mmol) in THF (10 mL). The mixture was stirred for 2 d. Solvent was removed, the deep brown oily residue was dissolved in benzene (10 mL), and the solution was filtered. Addition of $Pr^i{}_2NHCMe_2$ (0.18 g, 1.0 mmol) to the brown filtrate resulted in formation of a brown suspension. The mixture was stirred for 2 d and filtered. The product was crystallized by vapor diffusion of *n*-hexane, affording a black crystalline solid (0.11 g, 50%). The ^{1}H NMR spectrum was identical with that of the product from Method A.

Method C—The compound can also be prepared by reaction of double cubane [$Fe_8S_8(Pr^i{}_3P)_6$][23] or tetracubane [$Fe_{16}S_{16}(Pr^i{}_3P)_8$][22,23] with 6 or 12 equiv of $Pr^i{}_2NHCMe_2$, respectively, in benzene. Reactions were monitored by ^{1}H NMR; a typical procedure is given. To a solution of [$Fe_8S_8(Pr^i{}_3P)_6$] (51 mg, 0.030 mmol) in C_6D_6 (0.4 mL) was added $Pr^i{}_2NHCMe_2$ (3.3 mg, 0.18 mmol). After 2 h, the spectrum was identical to that of the product from Method A, demonstrating complete substitution of phosphine by the carbene.

[$Fe_4S_4(Pr^i{}_2NHCMe_2)_4$]

Method A—To a solution of [$FeCl_2$-$(PPr^i{}_3)_2$] (0.45 g, 1.00 mmol) in THF (10 mL) was added a solution of $(Me_3Si)_2S$ (0.36 g, 2.00 mmol) in THF (10 mL). The reaction mixture was stirred for 2 d. Solvent was removed to give a deep brown oily residue, which was dissolved in benzene (10 mL) and the solution was filtered. Addition of a solution of $Pr^i{}_2NHCMe_2$ (0.40 g, 2.20 mmol) in benzene (3 mL) resulted in formation of a brown suspension, which was stirrred for 4 d. The reaction mixture was filtered. Vapor diffusion of *n*-hexane into the brown filtrate afforded the product as deep red crystals (0.19 g, 72%). ^{1}H NMR (C_6D_6): δ 19.43 (1), 12.45 (br, 2). Methine proton signals were not observed. *Anal. Calcd*. for $C_{44}H_{80}Fe_4N_8S_4$: C, 49.26; H, 7.52; Fe, 11.96; N, 10.44; S, 20.80. Found: C, 49.16; H, 7.47; Fe, 11.76; N, 10.41; S, 21.08.

Method B—A solution of [$Fe_8S_8(Pr^i{}_2NHCMe_2)_6$] (0.18 g, 0.10 mmol) in benzene (5 mL) was treated with a solution of $Pr^i{}_2NHCMe_2$ (0.054 g, 0.30 mmol) in benzene (3 mL). The reaction mixture was stirred for 2 d and filtered. Vapor diffusion of *n*-hexane into the reddish-brown filtrate yielded the product as deep red crystals (0.14 g, 63%). The ^{1}H NMR spectrum was identical with that of the product from Method A.

Method C—The compound can be prepared by reaction of [$Fe_8S_8(Pr^i{}_3P)_6$] or [$Fe_{16}S_{16}(Pr^i{}_3P)_8$] with 8 or 16 equiv of $Pr^i{}_2NHCMe_2$, respectively, in benzene. The reactions are slow at room temperature, requiring *ca.* 2 d for completion, but the conversions are quantitative. At shorter reaction times, both [$Fe_4S_4(Pr^i{}_2NHCMe_2)_4$] and [$Fe_8S_8(Pr^i{}_2NHCMe_2)_6$] were observed by ^{1}H NMR.

X-Ray Structure Determinations

The structures of the three compounds in Table 1 were determined. Crystals of [$Fe_7S_6(PEt_3)_5Cl_2$] were grown by hexane diffusion into a THF solution. Crystals of [$Fe_8S_8(Pr^i{}_2NHCMe_2)_6$] and [$Fe_4S_4(Pr^i{}_2NHCMe_2)_4$] were obtained by hexane diffusion into

benzene solutions. Crystallizations were performed at room temperature. Crystals were coated with Paratone-N oil and mounted on a Bruker APEX CCD-based diffractometer equipped with an Oxford 700 low-temperature apparatus operating at 193 K. Data were collected with scans of 0.3 s/frame for 30 s. Cell parameters were retrieved with SMART software and refined using SAINT software on all reflections. Data integration was performed with SAINT, which corrects for Lorentz polarization and decay. Absorption corrections were applied using SADABS. Space groups were assigned unambiguously by analysis of symmetry and systematic absences determined by XPREP. All structures were solved and refined using SHELXTL software. The positions of metal atoms and their first coordination spheres were located from direct-methods *E*-maps; other non-hydrogen atoms were found in alternating difference Fourier syntheses and least-squares refinement cycles and during final cycles were refined anisotropically. Hydrogen atoms were placed in calculated positions employing a riding model. Final crystal parameters and agreement factors are reported in Table 1.[27]

Other Physical Measurements

All measurements were performed under anaerobic conditions. Absorption spectra were recorded with a Varian Cary 50 Bio spectrophotometer. ^{1}H NMR spectra were obtained with a Varian AM-400 spectrometer. Electrochemical measurements were made with a BioAnalytical Systems Epsilon potentiostat/galvanostat in THF solutions. Cyclic voltammetry measurements (50 mV/s) utilized a glassy carbon electrode and 0.1 M $(Bu_4N)(PF_6)$ supporting electrolyte. Under these conditions, $E_{1/2}$ = 0.55 V for the $[Cp_2Fe]^{0,1+}$ couple. Controlled potential electrolysis was performed with a BASi bulk electrolysis cell (glassy carbon felt) and 0.2 M supporting electrolyte. Potentials are referenced to the SCE. Iron-57 Mössbauer spectra were measured with a constant acceleration spectrometer. Data were analyzed with WMOSS software (Web Research Corp., Edina, MN). Isomer shifts are relative to iron metal at room temperature.

In the sections that follow, compounds are designated **1**–**8** according to the Chart 1.

Results and Discussion

The conclusion that all-ferrous clusters $[Fe_4S_4(PR_3)_4]^0$ (R = Pr^i, Bu^t, Cy) generated by chemical reduction of $[Fe_4S_4(PR_3)_4]^{1+}$ have at least transitory existence in THF solutions[22,23] before converting to higher nuclearity clusters by phosphine dissociation suggested a synthetic approach utilizing another neutral ligand type with more pronounced binding tendencies. Target clusters are preferably neutral rather than anionic to promote oxidative stability and thus require an uncharged terminal ligand. *N*-Heterocyclic carbenes[28,29] are generally considered similar to tertiary phosphines but are stronger electron donors with variable π-acceptor properties.[30–32] Further, NHCs have been demonstrated to bind to Fe^{II} in stable (nonorganometallic) compounds.[33–36] As shown here, the carbene Pr$^i_2$NHCMe$_2$ is entirely suitable for the purpose at hand. Syntheses leading to cubane-type clusters **4** and **5** are described first, followed by structures and other properties.

Cluster Synthesis

The synthetic scheme, set out in Figure 1, is based on reactions of **1** or **2** as a soluble Fe^{II} source in THF, $(Me_3Si)_2S$ as a sulfide source and chloride acceptor, and the carbene. Reactions were carried out in THF or benzene. All new compounds were identified by X-ray structure determinations.

(a) [Fe$_8$S$_8$(Pr$^i_2$NHCMe$_2$)$_6$]—In initial experiments, reaction of **1** with 1.5 equiv of $(Me_3Si)_2S$ afforded the black all-ferrous heptanuclear cluster **3** (70%). When **3** is used as a soluble polynuclear Fe^{II} precursor in a reaction system containing 5 equiv of Pr$^i_2$NHCMe$_2$,

the crystalline black double cubane **4** (52%) is obtained. As shown in Figure 1, this compound can also be prepared by two other methods. Reaction of **2** with excess $(Me_3Si)_2S$ (2 equiv) followed by 1 equiv of $Pr^i_2NHCMe_2$ affords cluster **4** directly (50%) in the overall assembly reaction 2. In reactions monitored by ^1H NMR, stoichometric treatment of double cubane **6** with 6 equiv of carbene in reaction 3 and tetracubane **7** with 12 equiv of carbene affords complete substitution and formation of **4** after *ca.* 2 h. This cluster is readily identified by its distinctive NMR spectrum (vide infra). These reactions demonstrate the stronger binding by carbene over phosphine. Because the phosphine clusters are obtained by multistep syntheses,[23] reaction 2 is presently the method of choice for **4**.

$$8[FeCl_2(PPr^i_3)_2]+8(Me_3Si)_2S+6Pr^i_2NHCMe_2 \rightarrow [Fe_8S_8(Pr^i_2NHCMe_2)_6]+16Me_3SiCl+16PPr^i_3 \quad (2)$$

$$[Fe_8S_8(PPr^i_3)_6]+6Pr^i_2NHCMe_2 \rightarrow [Fe_8S_8(Pr^i_2NHCMe_2)_6]+6PPr^i_3 \quad (3)$$

(b) $[Fe_4S_4(Pr^i_2NHCMe_2)_4]$—Single cubane cluster **5** is accessible by three routes (Figure 1). Assembly reaction 4, carried out with a sufficient amount of carbene (2.2 equiv) to cleave any intermediate double cubane, affords the product as a deep red crystalline solid. The reaction system requires ≥4 d, but the long reaction time is compensated by a favorable yield (72%). The cluster is also obtained by cleavage reaction 5 of the preisolated double cubane (63%). In reactions analogous to reaction 3 and examined by ^1H NMR, phosphine clusters **6** and **7** are converted to **5** with 8 or 16 equiv of $Pr^i_2NHCMe_2$, respectively. The additional equivs of carbene are required for cleavage of substituted double- or tetracubane to the single cubane in slow reactions (*ca.* 2 d) which, however, produce quantitative conversions. Clusters **4** and **5** are readily distinguished by their NMR spectra.

$$4[FeCl_2(PPr^i_3)_2]+4(Me_3Si)_2S+4Pr^i_2NHCMe_2 \rightarrow [Fe_4S_4(Pr^i_2NHCMe_2)_4]+8Me_3SiCl+8PPr^i_3 \quad (4)$$

$$[Fe_8S_8(Pr^i_2NHCMe_2)_6]+2Pr^i_2NHCMe_2 \rightarrow 2[Fe_4S_4(Pr^i_2NHCMe_2)_4] \quad (5)$$

Molecular Features of Carbene Clusters

(a) $[Fe_8S_8(Pr^i_2NHCMe_2)_6]$

(i) Solid State: Our first attempts to prepare fully reduced iron–sulfur clusters centered on the reaction of **1** and $(Me_3Si)_2S$, with the intent to obtain a polynuclear precursor cluster. The species isolated was all-ferrous cluster **3** whose structure is shown in Figure 2. This compound is structurally and metrically similar to previously reported $[Fe_7S_6(PEt_3)_4Cl_3]$,[37] which, however, contains one Fe^{III} atom. Cluster **3** is only the second example among the large structural diversity of iron–sulfur clusters[38] of monocapped prismane stereochemistry, here with Fe(1) as the capping atom. The cluster has idealized C_s symmetry with the mirror plane containing core atoms Fe(1,4,5)S(1,5); interatomic distances are averaged under this symmetry in Table 2. Another conspicuous feature of the cluster is the different geometries at sites with terminal chloride and phosphine ligands, illustrated by metric data for two such sites. For the Fe(2)-S_3Cl site, the angles S–Fe–S < Cl–Fe–S, the Fe atom is displaced 0.984(2) Å from the S_3 plane, and a distorted tetrahedral stereochemistry is apparent. The Fe(1)-S_3P site, on the other hand, displays the angles S–Fe–S > P–Fe–S, a smaller Fe atom displacement of 0.360(2) Å from the S_3 plane, and trigonal pyramidal stereochemistry. The latter arrangement is unusual but is precedented in a small number of Fe–S–P clusters including $[Fe_6S_6(PR_3)_4L_2]$ (R = Et, Bu^n; L = halide, RS^-),[39,40] and is associated with phosphines having cone angles ≤140°. The isolation of **3** enabled a subsequent reaction with carbene to yield the double cubane **4**. When

2 was used as the Fe^{II} source, the intermediate(s) prior to addition of carbene could not be isolated but with the carbene present reaction 2 proceeds.

As seen in Figure 3, the structure of **4** presents the edge-bridged double cubane motif established for **6**, $[Fe_8S_8(PCy_3)_6]$, and $[Fe_8S_8(Pr^i_3P)_4(SSiPh_3)_2]$.[22,23] Characteristic features include centrosymmetry and idealized C_{2h} symmetry of the Fe_8S_8 core, distorted tetrahedral FeS_3C and FeS_4 sites, a Fe_2S_2 bridge rhomb with the intercubane Fe(1)–S(1) distance (2.303 (2) Å) shorter than the intracubane Fe(1)-S(1A) distance (2.435(1) Å) but comparable with the mean value of other cubane distances (2.32(1) Å), an Fe(1)-Fe(1A) separation (2.862 Å) substantially longer than Fe–Fe cubane distances, and a cubane face adjacent to the bridge rhomb distorted relative to other faces by a short Fe(1)–Fe(4) distance (2.554(1) Å). The mean Fe–C bond length (2.10(4) Å) accords with the few available data for tetrahedral Fe^{II}–C bonds (2.12–2.14 Å),[33,36] and is longer than bonds to six-coordinate low-spin Fe^{II} (1.91–1.96 Å).[34,35] Compiled structure data are shown in Table 3.

The zero-field ^{57}Fe Mössbauer spectrum of polycrystalline **4**, shown in Figure 4, is well resolved and, consistent with the cluster structure, consists of three quadrupole doublets in a 2:1:1 intensity ratio. The spectra were fit with the parameters in Table 4. The most intense doublet is associated with the four sites off the idealized mirror plane and the other doublets with pairs of sites on this plane. The mean isomer shift $\delta_{av} = 0.62$ mm/s requires an all-ferrous formulation and is essentially identical with mean value $\delta_{av} = 0.60$ mm/s for phosphine-ligated **6**.

(ii) Solution State: Cluster **4** is freely soluble in benzene, toluene, and THF, in which solvents the ^{1}H NMR spectra are practically identical. Carbene-substituted iron sites are in a 2:1 ratio, with two sites *m* (Fe(3,3A)) on the mirror plane and the other four sites *m′* off the plane. The spectrum of **4**, displayed in Figure 5, is isotropically shifted because of cluster paramagnetism and consists of a broad methine signal at −2.34 ppm and five methyl signals at 0.40–7.11 ppm. That at 2.08 ppm has half the intensity of the others; the relative intensity of the 7.11 ppm signal was taken from the spectrum in THF-d_8. Ligands at the two sites give rise to isopropyl and olefinic methyl resonances in 2:1 intensity ratio, with the signals from the *m′* sites twice as intense as from the *m* sites. However, the *m′* isopropyl methyl groups are diastereotopic (as in **6**[23] and other edge-bridged double cubanes[41]). Consequently, the *m* (1, 2) and *m′* (2, 2, 2) ligands should generate five methyl signals with the indicated relative intensities, as observed, with that at 2.08 ppm due to the olefinic methyl groups at *m.* The spectra in toluene at 193–313 K showed increasing downfield shifts with decreasing temperature but no features indicative Fe–C hindered ligand rotation or other dynamical process. Demonstration of the structure of **4** in solution is necessary to authenticate reaction 5.

(b) $[Fe_4S_4(Pr^i_2NHCMe_2)_4]$

(i) Solid State: The structure of cluster **5** provided in Figure 6 reveals the cubane-type sterechemistry of the $[Fe_4S_4]^0$ core. Metric data are collected in Table 5 and structural comparisons with **8** and the cluster in *Av* Fe protein are found in Table 6. The iron sites have distorted tetrahedral FeS_3C coordination and planar Fe-carbene units of essentially identical dimensions. The mean Fe–C bond length of 2.10(3) Å is the same as that of **4**; representative metric data for one carbene ligand are given.

No symmetry is imposed on the cluster and there are no systematic distortions toward an idealized core symmetry evident in the Fe–S and Fe–Fe distances. A number of $[Fe_4S_4]^{2+}$ clusters, for example, exhibit a compressed tetragonal (D_{2d}) distortion.[17] Mean Fe–S and Fe–Fe distances compare closely among the three fully reduced clusters. The distribution and range of Fe–Fe distances in **5** more closely resembles **8** than those derived from crystallographic and EXAFS analyses of the *Av* Fe protein. The X-ray data suggest one long, one short, and four

intermediate Fe–Fe distances with a range of 0.25 Å,[10] while the best fit of EXAFS results occurs with values of 2.52 Å and 2.77 Å in a 2:1 ratio.[8] No such bias in Fe–Fe distances is found with **5**, in which the distance range is 0.16 Å.[8] Core component (Fe_4, S_4) and total (Fe_4S_4) volumes tend to increase slightly with reduction as electrons are added to antibonding orbitals and the Fe^{II} core character increases. For example, V(Fe_4S_4) increases by 0.25 $Å^3$ (R = CH_2Ph) and 0.18 $Å^3$ (R = Ph) in the pairs $[Fe_4S_4(SR)_4]^{2-,3-}$,[42] but is much smaller (0.07 $Å^3$) in $[Fe_4S_4(CN)_4]^{3-,4-}$. The same trend is not clearly evident in protein-bound $[Fe_4S_4]^{2+,0}$ clusters,[10] but uncertainties in calculated volumes have not been given. On the basis of limited current information, we conclude that the $[Fe_4S_4]^0$ cores **5** and **8** are nearly congruent and are less distorted versions of the cluster in *Av* Fe protein.[43]

The Mössbauer spectrum of polycrystalline **5** at 77 K (Figure 4) has been analyzed in terms of two quadrupole doublets in a 3:1 intensity ratio with quadrupole splittings ΔE_Q = 2.92 mm/s for the less intense and 1.54 mm/s for the more intense doublet. The isomer shift δ_{av} = 0.61 mm/s confirms the all-ferrous formulation and compares closely with the other values in Table 4. The zero-field spectrum of the Ti^{III}(citrate)-reduced *Av* Fe protein at 4.2 and 130 K has an appearance quite similar to the spectrum in Figure 4 and has been analyzed in terms of four equally intense quadrupole doublets, all with δ = 0.68 mm/s.[9] At 130 K, the less intense resolved doublet has ΔE_Q = 2.91 mm/s and the overlapping doublets ΔE_Q = 1.05, 1.45, 1.70 mm/s. The close electronic relationship between **5** and the protein-bound cluster based on Mössbauer spectra is clearly evident.

(ii) Solution State: The solubility properties of **5** are very similar to those of **4**. The cluster is stable in aprotic solvents under anaerobic conditions for at least 3–4 days. The isotropically shifted ^1H NMR spectrum in benzene (Figure 5) consists of two resonances in a 1:2 intensity ratio, olefinic methyl groups at 19.4 ppm and isopropyl methyl groups at 12.5 ppm; methine protons were not detected. Note the absence of diastereotopic methyl resonances; the spectrum is consistent with the solid state structure.

The absorption spectra of both clusters in benzene are shown in Figure 7. Cluster **4** forms a brown solution with a band at 380 nm and a second unresolved feature at 562 nm. Cluster **5** forms a red solution with a shoulder at 368 nm and a broad but discernible absorption near 510 nm. The latter feature is of potential interest because aqueous buffer solutions of Ti^{III}(citrate)-reduced *Av* Fe protein are red and display a band at 520 nm which has been suggested as a signature of a $[Fe_4S_4]^0$ cluster in protein.[6] Further credence to this possibility is offered by the 518 nm band observed for **8** in acetonitrile/THF in the presence of excess reductant.[24] Given the transparency of the carbene ligand (Figure 7) and a minor dependence on terminal ligand, this transition appears to be confined to the cluster core.

The oxidative stability of cluster **5** in THF solution was examined by cyclic voltammetry. The cluster undergoes two oxidations at $E_{1/2}$ = −1.30 V and *ca.* −0.89 V shown in the voltammogram in Figure 8. When scanned separately, the first process is chemically reversible with $i_a/i_c \approx 1$. Controlled potential coulometry at −1.0 V yielded n = 1.00(9) e^-, establishing the redox couple as $[Fe_4S_4(Pr^i{}_2NHCMe_2)_4]^{0/1+}$. The potential for this couple is lower than that might have been expected,[43] but not as negative as those given at the outset for the strongly anionic couples $[Fe_4S_4(CN)_4]^{4-/3-}$ and $[Fe_4S_4(SR)_4]^{4-/3-}$. The low potential in the absence of net negative cluster charge is most likely a consequence of the pronounced σ-donor propensity of carbene ligands.

Summary

The following are the principal results and conclusions of this investigation.

1. Fully reduced iron-sulfur-carbene clusters of nuclearities eight and four can each be prepared by three methods: $[Fe_8S_8(Pr^i{}_2NHCMe_2)_6]$ from an Fe_7 precursor, by self-assembly, and by phosphine subsitution of Fe_8S_8 and $Fe_{16}S_{16}$ clusters; $[Fe_4S_4(Pr^i{}_2NHCMe_2)_4]$ by self-assembly, phosphine substitution, and cleavage of $[Fe_8S_8(Pr^i{}_2NHCMe_2)_6]$.
2. The phosphine substitution reactions in (1) reveal the carbene to be a stronger electron donor than a tertiary alkylphosphine, at least toward tetrahedral Fe^{II}.
3. $[Fe_8S_8(Pr^i{}_2NHCMe_2)_6]$ has the edge-bridged double cubane structure previously stabilized only with phosphines ($[Fe_8S_8(PR_3)_6]$[22,23] and isonitriles ($[Fe_8S_8(RNC)_{18}]^{2+}$, two-electron oxidized core, octahedral metal sites[44]).
4. $[Fe_4S_4(Pr^i{}_2NHCMe_2)_4]$ has a cubane-type structure in which the all-ferrous state has been previously isolated only as the highly unstable $[Fe_4S_4(CN)_4]$[4–24] and as $[Fe_4S_4(S_{Cys})_4]$ in the *Av* Fe protein of nitrogenase.[5–11] Structural parameters and the ^{57}Fe isomer shift are fully consistent with the all-ferrous formulation. The cluster core is an accurate synthetic analogue of the protein-bound $[Fe_4S_4]^0$ core.
5. The two clusters are the first examples of (nonorgano-metallic) iron–sulfur clusters with Fe–C bonds.
6. The low redox potential of the $[Fe_4S_4(Pr^i{}_2NHCMe_2)_4]^{0/1+}$ couple (−1.30 V in THF) notwithstanding, the neutral cluster is stable and manipulable in aprotic solutions under conventional anaerobic conditions in the absence of reductant, thereby enabling the first examination of the reactivity properties of the $[Fe_4S_4]^0$ state. The electronic and reactivity properties of this state are currently under investigation.

Supplemental Materials

Refer to Web version on PubMed Central for supplementary material.

Acknowledgements

This research was supported by NIH Grant GM 28856. We thank Dr. T. A. Scott for experimental assistance.

References

1. Beinert H, Holm RH, Münck E. Science 1997;277:653–659. [PubMed: 9235882]
2. Noodleman L, Lovell T, Liu T, Himo F, Torres RA. Curr Opin Chem Biol 2002;6:259–273. [PubMed: 12039013]
3. Johnson DC, Dean DR, Smith AD, Johnson MK. Annu Rev Biochem 2005;74:247–281. [PubMed: 15952888]
4. Howard JB, Rees DC. Chem Rev 1996;96:2965–2982. [PubMed: 11848848]
5. Watt GD, Reddy KRN. J Inorg Biochem 1994;53:281–294.
6. Angove HC, Yoo SJ, Burgess BK, Münck E. J Am Chem Soc 1997;119:8730–8731.
7. Yoo SJ, Angove HC, Burgess BK, Münck E, Peterson J. J Am Chem Soc 1998;120:9704–9705.
8. Musgrave KB, Angove HC, Burgess BK, Hedman B, Hodgson KO. J Am Chem Soc 1998;120:5325–5326.
9. Yoo SJ, Angove HC, Burgess BK, Hendrich MP, Münck E. J Am Chem Soc 1999;121:2534–2545.
10. Strop P, Takahara PM, Chiu HJ, Angove HC, Burgess BK, Rees DC. Biochemistry 2001;40:651–656. [PubMed: 11170381]
11. Guo M, Sulc F, Ribbe MW, Farmer PJ, Burgess BK. J Am Chem Soc 2002;124:12100–12101. [PubMed: 12371842]

12. Abbreviations: *Av*, *Azotobacter vinelandii*; Cy, cyclohexyl; Me_2NHCMe_2, 1,3,4,5-tetramethylimidazol-2-ylidene; NHE, normal hydrogen electrode; SCE, saturated calomel electrode; NHC, N-heterocyclic carbene; $Pr^i_2NHCMe_2$, 1,3-diisopropyl-4,5-dimethylimi-dazol-2-ylidene.
13. Angove HC, Yoo SJ, Münck E, Burgess BK. J Biol Chem 1998;273:26330–26337. [PubMed: 9756863]
14. Nyborg AC, Johnson JL, Gunn A, Watt GD. J Biol Chem 2000;275:39307–39312. [PubMed: 11005818]
15. Howard JB, Rees DC. Proc Natl Acad Sci USA 2006;103:17088–17093. [PubMed: 17088547]
16. Lowery TJ, Wilson PE, Zhang B, Bunker J, Harrison RG, Nyborg AC, Thiriot D, Watt GD. Proc Natl Acad Sci USA 2006;103:17131–17136. [PubMed: 17085583]
17. Rao PV, Holm RH. Chem Rev 2004;104:527–559. [PubMed: 14871134]
18. Zhou C, Raebiger JW, Segal BM, Holm RH. Inorg Chim Acta 2000;300–302:892–902.
19. DePamphilis BV, Averill BA, Herskovitz T, Que L Jr, Holm RH. J Am Chem Soc 1974;96:4159–4167. [PubMed: 4854591]
20. Cambray J, Lane RW, Wedd AG, Johnson RW, Holm RH. Inorg Chem 1977;16:2565–2571.
21. (a) Job RC, Bruice TC. Proc Natl Acad Sci USA 1975;72:2478–2482. [PubMed: 16592256] (b) Henderson RA, Sykes AG. Inorg Chem 1980;19:3103–3105. (c) Pickett CJ. J Chem Soc, Chem Commun 1985:323–324. (d) Ollerenshaw TJ, Garner CD, Odell B, Clegg W. J Chem Soc Dalton Trans 1985:2161–2165.
22. Goh C, Segal BM, Huang J, Long JR, Holm RH. J Am Chem Soc 1996;118:11844–11853.
23. Zhou HC, Holm RH. Inorg Chem 2003;42:11–21. [PubMed: 12513073]
24. Scott TA, Berlinguette CP, Holm RH, Zhou HC. Proc Natl Acad Sci USA 2005;102:9741–9744. [PubMed: 15985547]
25. Booth G, Chatt J. J Chem Soc 1962:2099–2106.
26. Kuhn N, Kratz T. Synthesis 1993:561–562.
27. See Supporting Information.
28. Bourissou D, Guerret O, Gabbai FP, Bertrand G. Chem Rev 2000;100:39–91. [PubMed: 11749234]
29. Herrmann WA. Angew Chem, Int Ed 2002;41:1290–1309.
30. Chianese AR, Kovacecic A, Zeglis BM, Faller JW, Crabtree RH. Organometallics 2004;23:2461–2468.
31. Khramov DM, Lynch VM, Bielawski CW. Organometallics 2007;26:6042–6049.
32. Kausamo A, Tuononen HM, Krahulic KE, Roesler R. Inorg Chem 2008;47:1145–1154. [PubMed: 18166046]
33. Louie J, Grubbs RH. Chem Commun 2000:1479–1480.
34. Danopoulos AA, Tsoureas N, Wright JA, Light ME. Organometallics 2004;23:166–168.
35. McGuinness DS, Gibson VC, Steed JW. Organometallics 2004;23:6288–6292.
36. Nieto I, Cervantes-Lee F, Smith JM. Chem Commun 2005:3811–3813.
37. Noda I, Snyder BS, Holm RH. Inorg Chem 1986;25:3851–3853.
38. Holm, RH. Iron-Sulfur Clusters. In: Que, L., Jr; Tolman, WA., editors. Bio-coordination Chemistry. Elsevier; Oxford: 2004. p. 61-90.
39. Snyder BS, Holm RH. Inorg Chem 1988;27:2339–2347.
40. Reynolds MS, Holm RH. Inorg Chem 1988;27:4494–4499.
41. Osterloh F, Segal BM, Achim C, Holm RH. Inorg Chem 2000;39:980–989. [PubMed: 12526378]
42. Berg, JM.; Holm, RH. Structures and Reactions of Iron-Sulfur Protein Clusters and Their Synthetic Analogues. In: Spiro, TG., editor. Iron-Sulfur Proteins. Chapter 1. Wiley-Interscience; New York: 1982.
43. We have also prepared and determined the structure of $[Fe_4S_4(Me_2NHCMe_2)_4]$. This cluster does not show any systematic distortion and is isostructural and nearly isometric with 5 (mean values, Å: Fe–S 2.33(2), Fe–Fe 2.67(4), Fe–C 2.09(2)); Deng, L.; Holm, R. H., results to be published. The structure of 5 is not significantly influenced by any intramolecular steric interactions involving isopropyl groups. In THF, $E_{1/2} = -1.34$ V for the $[Fe_4S_4(Me_2NHCMe_2)_4]^{0/1+}$ couple.
44. Harmjanz M, Saak W, Pohl S. J Chem Soc, Chem Commun 1997:951–952.

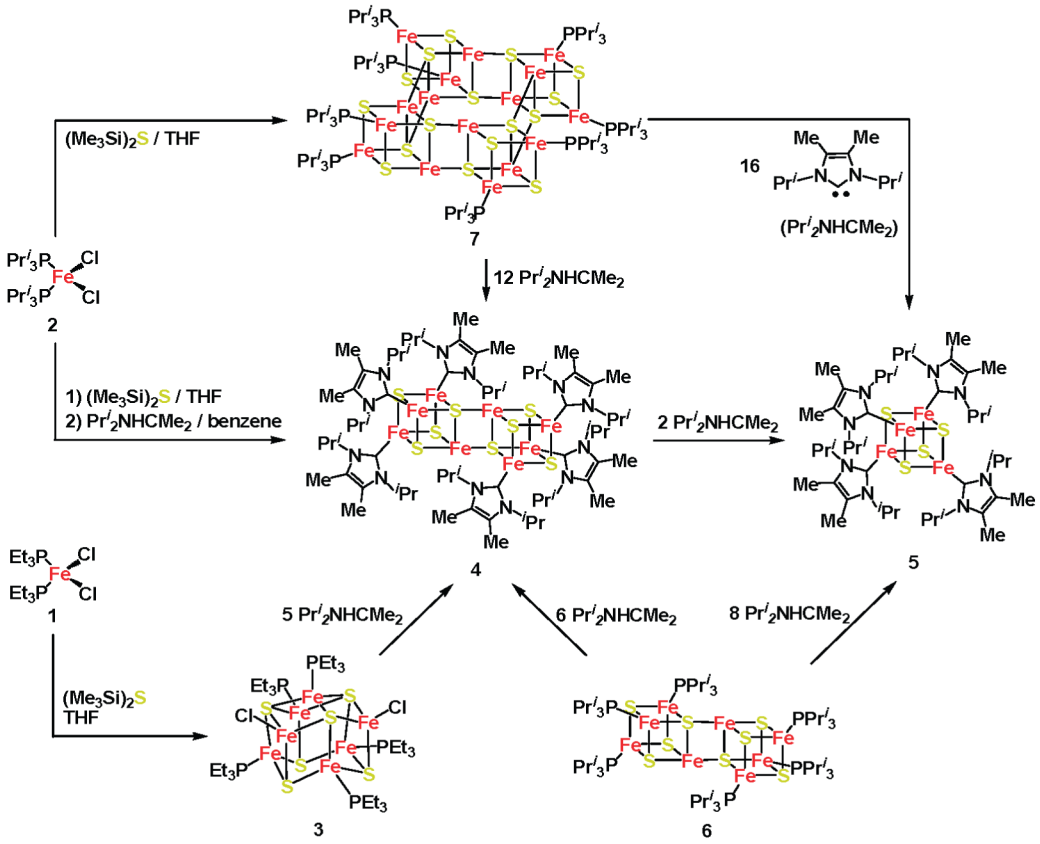

Figure 1.

Synthesis and conversion reactions of all-ferrous iron–sulfur clusters **3**–**7** derived from Fe^{II} precursors **1** and **2** and $(Me_3Si)_2S$ as the sulfur source.

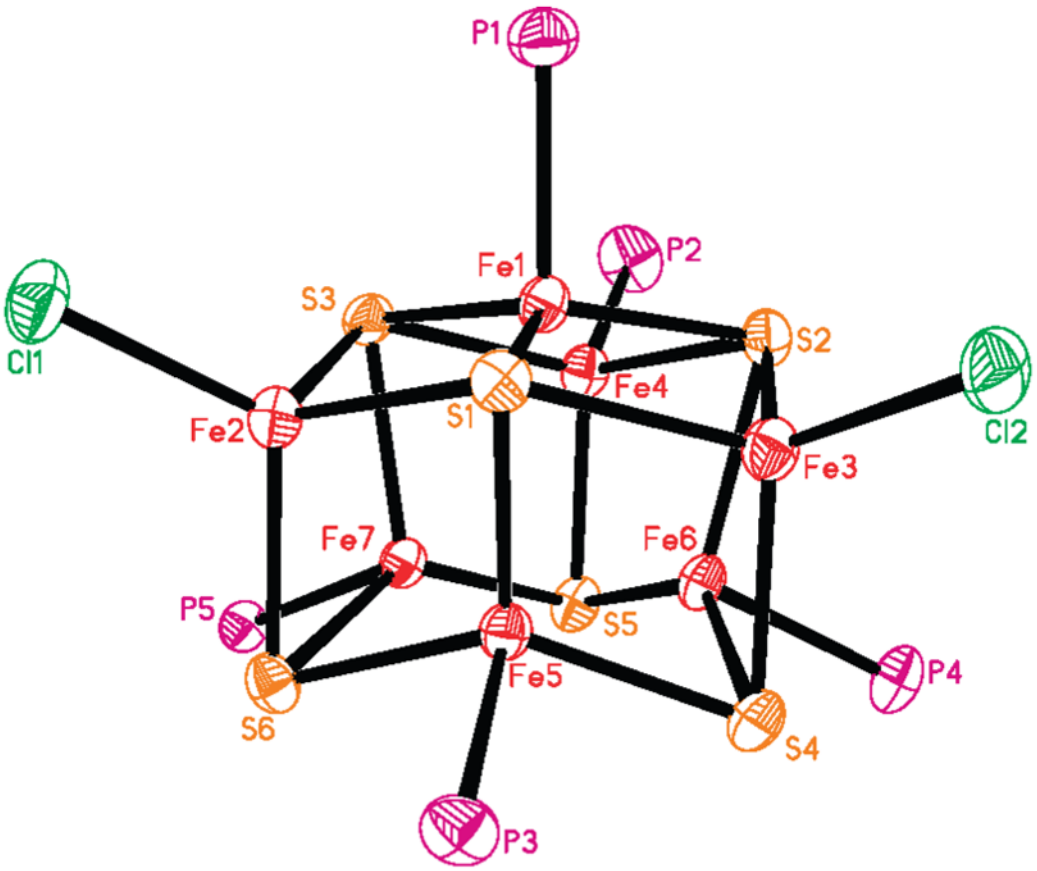

Figure 2.
Structure of $[Fe_7S_6(PEt_3)_5Cl_2]$ showing 30% probability ellipsoids. For clarity, the ethyl groups are omitted.

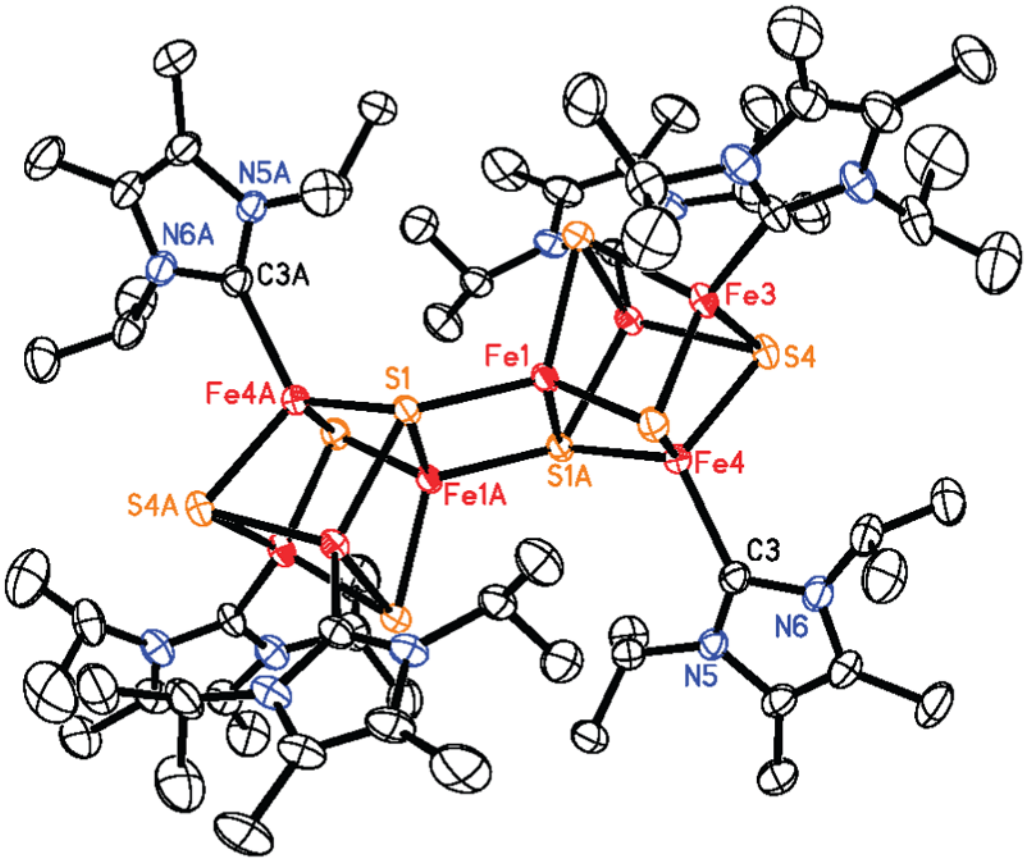

Figure 3.
Structure of $[Fe_8S_8(Pr^i_2NHCMe_2)_6]$ showing 30% probability ellipsoids and a partial atom labeling scheme. Atoms *n* and *n*A are related by imposed centrosymmetry.

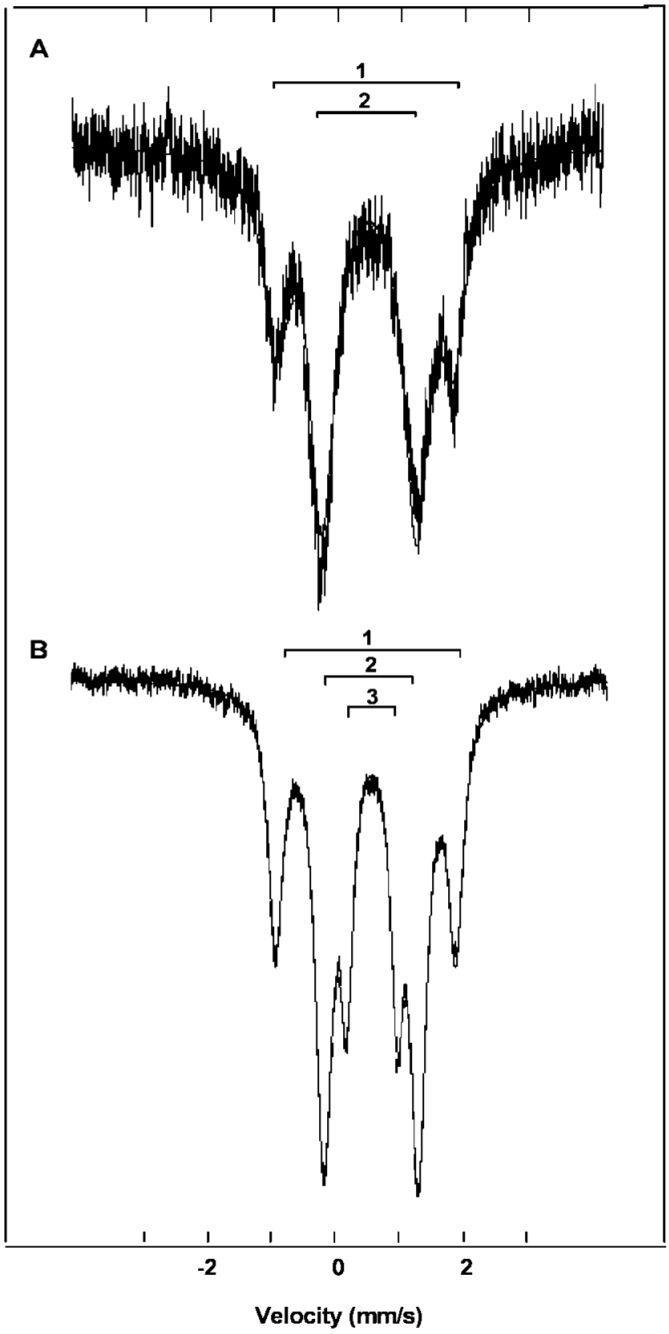

Figure 4.
Mössbauer spectra of polycrystalline $[Fe_4S_4(Pr^i_2NHCMe_2)_4]$ (A, at 77 K) and $[Fe_8S_8(Pr^i_2NHCMe_2)_6]$ (B, at 4.2 K). The spectra were fitted using the parameters of Table 4.

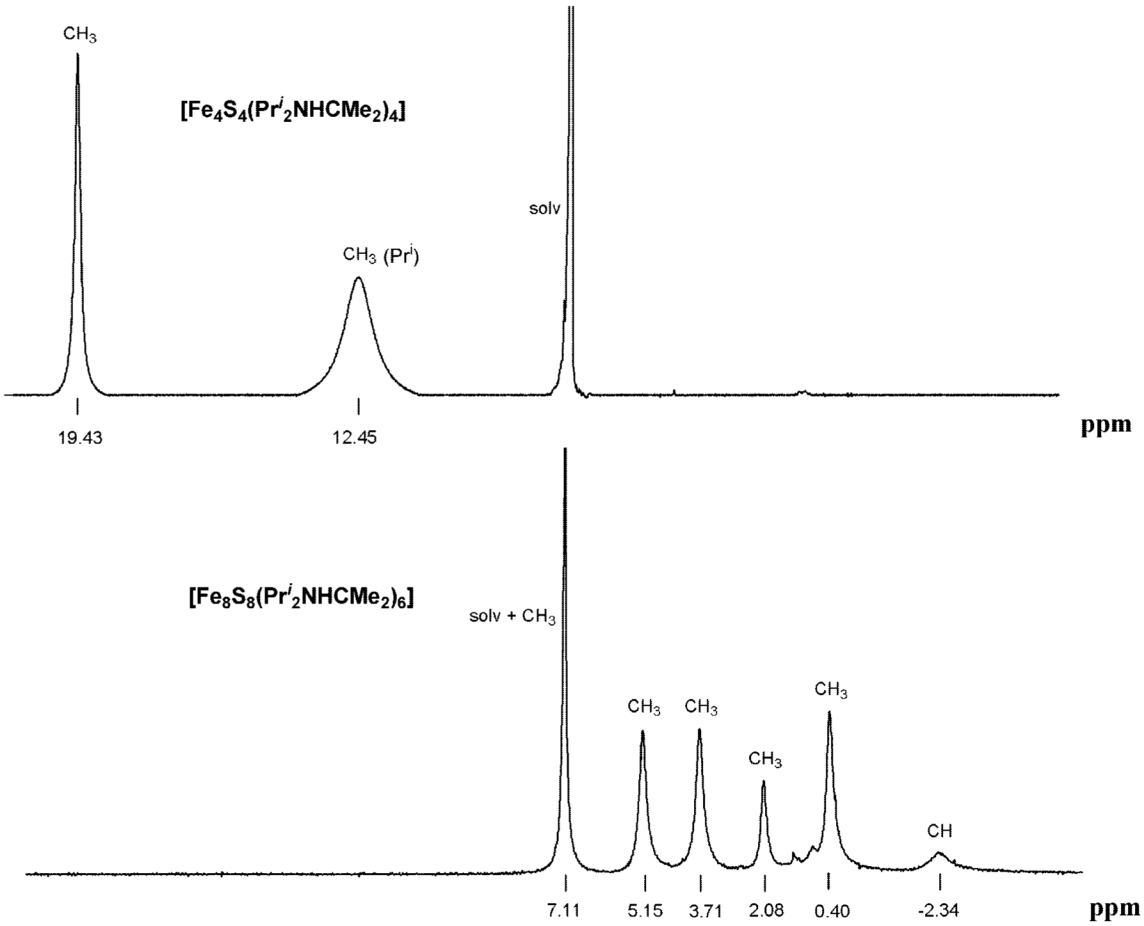

Figure 5.

^{1}H NMR spectra of [$Fe_4S_4(Pr^i{}_2NHCMe_2)_4$] (upper), [$Fe_8S_8(Pr^i{}_2NHCMe_2)_6$] (lower), in C_6D_6 at room temperature. The signals of one set of ligand methyl groups of [$Fe_8S_8(Pr^i{}_2NHCMe_2)_6$] and solvent overlap at 7.11 ppm.

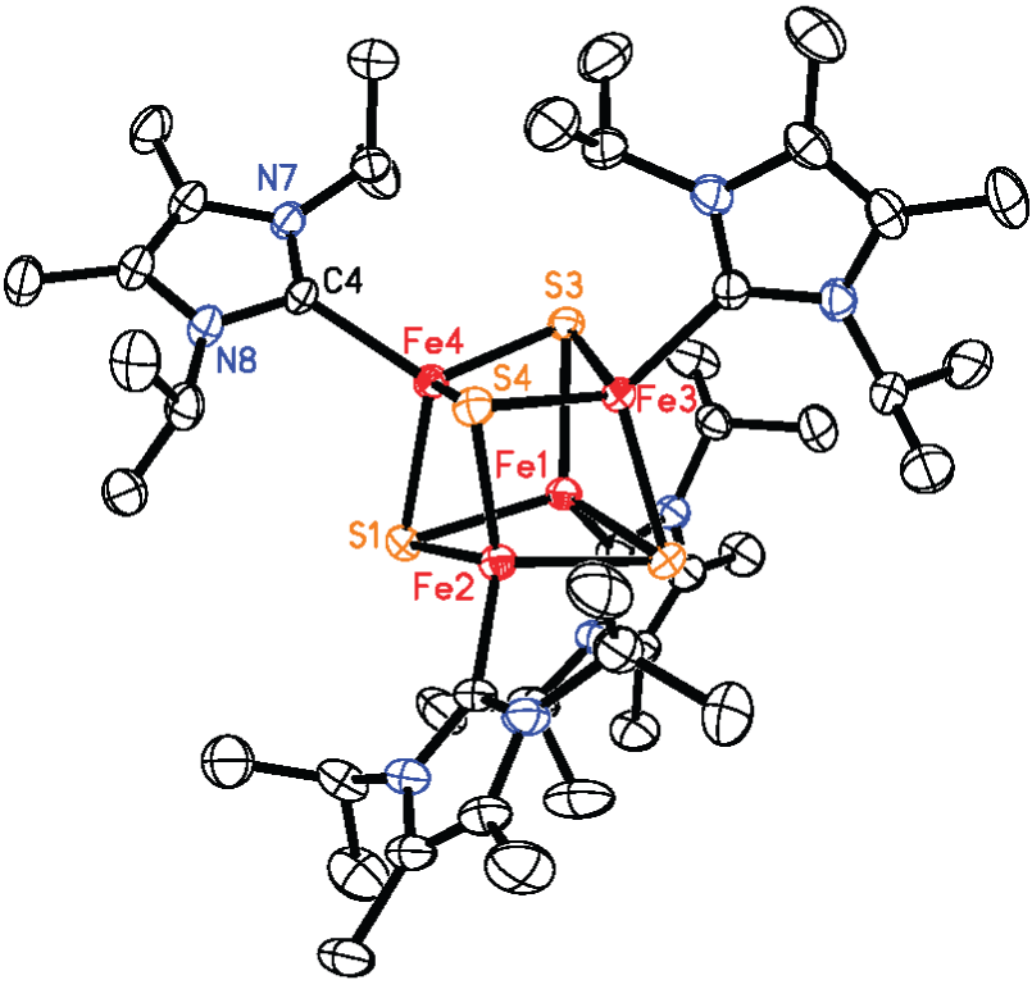

Figure 6.
Structure of $[Fe_4S_4(Pr^i{}_2NHCMe_2)_4]$ showing 30% probability ellipsoids and a partial atom labeling scheme.

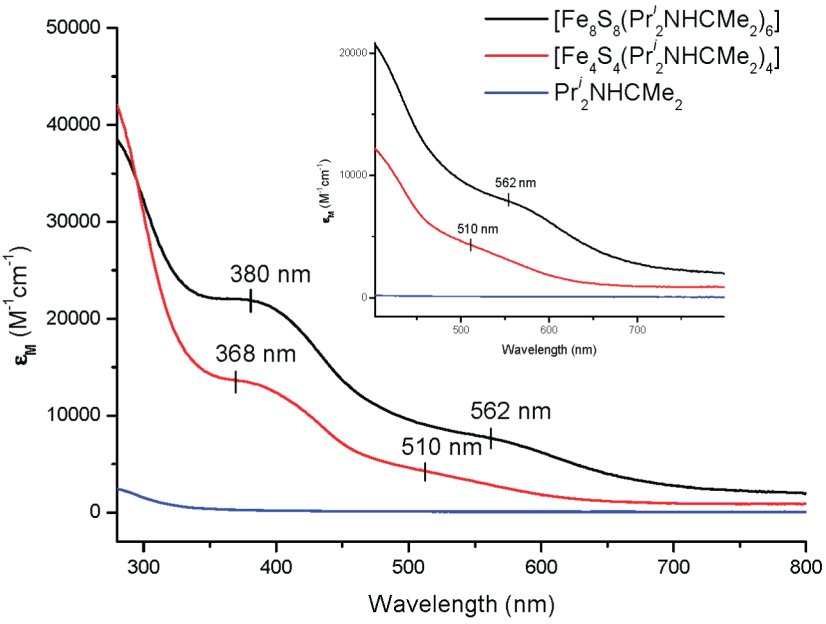

Figure 7.
UV– visible absorption spectra in benzene of $[Fe_4S_4(Pr^i{}_2NHCMe_2)_4]$ (red), $[Fe_8S_8(Pr^i{}_2NHCMe_2)_6]$ (black), and free ligand $Pr^i{}_2NHCMe_2$ (blue). (Inset) Enlarged absorption spectra between 400 and 800 nm.

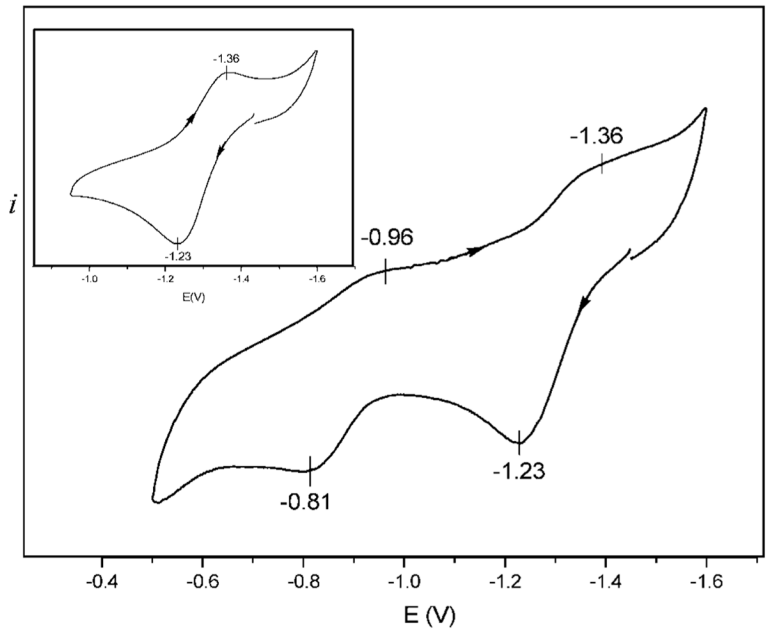

Figure 8.

Cyclic voltammograms (50 mV/s) of 3.7 mM $[Fe_4S_4(Pr^i{}_2NHCMe_2)_4]$ in THF with 0.10 M $(Bu^n{}_4N)(PF_6)$ supporting electrolyte. (Inset) Voltammogram at −1.0 to −1.6 V. Number peak potentials vs SCE are indicated.

$[Fe(R_3P)_2Cl_2]$	R = Et **1**,[25] Pr^i **2**
$[Fe_7S_6(PEt_3)_5Cl_2]$	**3**
$[Fe_8S_8(Pr^i{}_2NHCMe_2)_6]$	**4**
$[Fe_4S_4(Pr^i{}_2NHCMe_2)_4]$	**5**
$[Fe_8S_8(Pr^i{}_3P)_6]$	**6**[23]
$[Fe_{16}S_{16}(Pr^i{}_3P)_8]$	**7**[22,23]
$[Fe_4S_4(CN)_4]^{4-}$	**8**[24]

Chart 1.
Designation of Compounds

Table 1

Crystal Data and Summary of Data Collection and Refinement for Clusters **3**, **4**, and **5**[a]

	3	**4**	**5**
Formula	$C_{30}H_{75}Cl_2P_5Fe_7S_6$	$C_{66}H_{120}N_{12}Fe_8S_8$	$C_{44}H_{80}N_8Fe_4S_4$
crystal system	triclinic	triclinic	monoclinic
fw	1244.96	1785.02	1072.80
space group	$P\bar{1}$	$P\bar{1}$	Cc
a, Å	12.213(3)	11.788(1)	14.470(2)
b, Å	12.858(3)	14.111(1)	20.703(4)
c, Å	17.607(4)	15.450(1)	18.767(3)
α, deg	98.337(4)	106.468(1)	90
β, deg	95.007(4)	95.791(1)	96.635(2)
γ, deg	100.011(4)	92.206(1)	90
V, Å^3	2676(1)	2445.9(2)	5585(2)
Z	2	1	4
d_{calcd}, g/cm^3	1.545	1.212	1.276
2θ range, deg	2.4 to 50.0	2.8 to 50.0	3.4 to 50.0
GOF (F^2)	0.982	1.113	1.035
$R1$[b]	0.0504/0.0618[de]	0.0511/0.0711[de]	0.0251/0.0255[de]
$wR2$[c]	0.1396/0.1476[de]	0.1892/0.2027[de]	0.0663/0.0666[de]

[a] Collected using Mo Kα radiation (λ = 0.71073 Å) at 193 K.

[b] $R1 = \Sigma\,[(F_O - F_C)]/\Sigma\,(F_O)$.

[c] $wR2 = \{\Sigma\,[w(F_O^2 - F_C^2)^2/\Sigma[w(F_O^2)^2]\}^{1/2}$.

[d] $I > 2\sigma(I)$.

[e] All data.

Table 2

Selected Interatomic Distances (Å)[a] and Angles (deg) of $[Fe_7S_6(PEt_3)_5Cl_2]$

Fe(1)–S(1)	2.220(1)	Fe(1)–Fe(4)	2.602(1)
Fe(1)–S(2,3)[b]	2.190(4)	Fe(1)–Fe(2,3)	2.55(2)
Fe(2,3)–S(1)	2.365(1)	Fe(1)–Fe(6,7)	2.969(2)
Fe(2,3)–S(3,2)[b]	2.436(9)	Fe(2,3)–Fe(7,6)	2.637(6)
Fe(2,3)–S(6,4)	2.279(1)	Fe(2,3)–Fe(5)	2.631(6)
Fe(4)–S(2,3)	2.265(1)	Fe(4)-Fe(6,7)	2.64(1)
Fe(4)–S(5)	2.238(1)	Fe(5)-Fe(6,7)	2.720(5)
Fe(5)–S(1)	2.248(1)	Fe(1)–P(1)	2.267(2)
Fe(5)-S(4,6)	2.198(6)	Fe(4)–P(2)	2.355(2)
Fe(6,7)–S(2,3.	2.23(1.	Fe(5)–P(3)	2.271(2)
Fe(6,7)–S(5)	2.199(2)	Fe(6,7)–P(4,5)	2.265(3)
Fe(6,7)–S(4,6.	2.189(4)	Fe(2,3)–Cl(1,2)	2.226(7)
Fe–S_3P Site		*Fe–S_3Cl Site*	
S(1)–Fe(1)–P(1)	96.98(6)	S(1)–Fe(2)–Cl(1)	113.13(6)
S(2)–Fe(1)–P(1)	101.88(6)	S(3)–Fe(2)–Cl(1)	113.66(6)
S(3)–Fe(1)–P(1)	99.71(6)	S(6)–Fe(2)–Cl(1)	117.19(6)
S(1)–Fe(1)–S(2)	119.76(6)	S(1)–Fe(2)–S(3)	105.39(5)
S(1)–Fe(1)–S(3)	121.21(5)	S(1)–Fe(2)–S(6)	103.70(5)
S(2)–Fe(1)–S(3)	111.08(5)	S(3)–Fe(2)–S(6)	102.40(5)
Fe(1) ··· S(1,2,3)[c]	0.360(2)	Fe(2) ··· S(1,3,6)[c]	0.984(2)

[a] Averaged under idealized C_S symmetry.

[b] Bond distance notation: Fe(*m*)–S(*x*,*y*) is the mean of Fe(*m*)–S(*x*) and Fe(*m*)–S(*y*); Fe(*m*,*n*)–S(*x*,*y*) is the mean of Fe(*m*)–S(*x*) and Fe(*n*)–S(*y*).

[c] Displacement (Å) of Fe atom from S_3 plane.

Table 3

Selected Interatomic Distances (Å) and Angles (deg) of $[Fe_8S_8(Pr^i_2NHCMe_2)_6]$

Fe(1)–S(2)	2.326(2)	Fe(1)–Fe(2)	2.614(1)
Fe(1)–S(3)	2.314(2)	Fe(1)–Fe(3)	2.767(1)
Fe(2)–S(3)	2.312(2)	Fe(1)–Fe(4)	2.554(1)
Fe(2)–S(4)	2.327(2)	Fe(2)–Fe(3)	2.750(1)
Fe(3)–S(2)	2.293(2)	Fe(2)–Fe(4)	2.696(1)
Fe(3)–S(3)	2.323(2)	Fe(3)–Fe(4)	2.776(1)
Fe(3)–S(4)	2.296(2)		
Fe(4)–S(2)	2.316(2)	Fe(2)–C(1)	2.134(6)
Fe(4)–S(4)	2.332(2)	Fe(3)–C(2)	2.058(6)
mean of 9	2.32(1)	Fe(4)–C(3)	2.102(6)
		mean of 3	2.10(4)
Fe(2)–S(1A)	2.372(2)		
Fe(4)–S(1A)	2.360(2)	Fe(1)–S(1A)–Fe(2)	65.88(5)
		Fe(1)–S(1A)–Fe(4)	64.36(4)
bridge		Fe(2)–S(1A)–Fe(4)	69.48(5)
Fe(1)–S(1)	2.303(2)	Fe(2)–S(1A)–Fe(1A)	127.69(7)
Fe(1)–S(1A)	2.435(2)	Fe(4)–S(1A)–Fe(1A)	121.08(7)
Fe(1)–Fe(1A)	2.862(2)		
Fe(1)–S(1)–Fe(1A)	74.27(5)	S–Fe–S[a]	102.21(6)–114.05(6)
S(1)–Fe(1)–S(1A)	105.73(5)	Fe–S–Fe[b]	66.76(5)–74.06(6)
		Fe–Fe–Fe[a]	54.87(3)–62.39(3)
		C–Fe–S[b]	106.5(2)–119.5(2)

[a] Fe_4S_4, range of 12.

[b] S(2,3,4) or Fe(2,3,4), range of 9.

Table 4

^{57}Fe Mössbauer Parameters for $[Fe_4S_4]^0$ and $[Fe_8S_8]^0$ Clusters

cluster	T (K)	δ(mm/s)[a]	ΔE_Q (mm/s)[b]	%
$[Fe_4S_4(Pr^i_2NHCMe_2)_4]$	77	0.54	2.92	25
		0.62	1.54	75
$[Fe_4S_4(CN)_4]^{4-}$[c]	77	0.65	2.00	50
		0.65	1.45	50
$[Fe_8S_8(PPr^i_3)_6]$[d]	4.2	0.53	2.49	25
		0.64	0.94	75
$[Fe_8S_8(Pr^i_2NHCMe_2)_6]$	4.2	0.55	2.93	25
		0.64	1.54	50
		0.65	0.82	25
Av Fe protein[e]	4.2	0.68[f]	3.08, 1.72	25
			1.48, 1.24	25

[a] Referenced to Fe metal at room temperature; ±0.02 mm/s.

[b] ±0.03 mm/s.

[c] Reference 23.

[d] Reference 22.

[e] References 6, 9.

[f] Spectrum analyzed as four equally intense doublets with the same isomer shift.

Table 5

Selected Interatomic Distances (Å) and Angles (deg) of $[Fe_4S_4(Pr^i_2NHCMe_2)_4]$

Fe(1)–S(1)	2.337(1)	Fe(1)–Fe(2)	2.719(1)
Fe(1)–S(2)	2.338(1)	Fe(1)–Fe(3)	2.603(1)
Fe(1)–S(3)	2.328(1)	Fe(1)–Fe(4)	2.675(1)
Fe(2)–S(1)	2.291(1)	Fe(2)–Fe(3)	2.710(1)
Fe(2)–S(2)	2.334(1)	Fe(2)–Fe(4)	2.764(1)
Fe(2)–S(4)	2.308(1)	Fe(3)–Fe(4)	2.613(1)
Fe(3)–S(2)	2.318(1)	mean of 6	2.68(6)
Fe(3)–S(3)	2.370(1)		
Fe(3)–S(4)	2.344(1)	Fe(1)–C(1)	2.125(2)
Fe(4)–S(1)	2.335(1)	Fe(2)–C(2)	2.058(6)
Fe(4)–S(3)	2.334(1)	Fe(3)–C(3)	2.102(6)
Fe(4)–S(4)	2.327(1)	Fe(4)–C(4)	2.127(2)
mean of 12	2.33(2)	mean of 4	2.10(3)
range of 12		*ligand*	
S–Fe–S	102.32(3)–110.69(3)	C(1)–N(1)	1.349(4)
Fe–S–Fe	68.00(2)–73.38(2)	C(1)–N(2)	1.354(3)
Fe–Fe–Fe	57.00(1)–62.55(2)	N(1)–C(12)	1.392(4)
C–Fe–S	105.43(8)–119.22(8)	N(2)–C(11)	1.402(3)
		C(11)–C(12)	1.347(4)
		N(1)–C(1)–N(2)	105.0(2)

Table 6

Comparison of Structural Parameters of Cubane-Type $[Fe_4S_4]^0$ Clusters

			Av Fe protein	
	$[Fe_4S_4(Pr^i_2NHCMe_2)_4]$	$[Fe_4S_4(CN)_4]^{4-}$ [a]	X-ray [b]	XAS [c]
Fe–Fe (Å)	2.764(1), 2.675(1) 2.719(1), 2.613(1) 2.710(1), 2.603(1)	2.676(1), 2.696(1) 2.683(1), 2.683(1) 2.627(1), 2.676(1)	2.79, 2.67 2.69, 2.57 2.66, 2.54	2.77, 2.53 2.77, 2.53 2.53, 2.53
mean	2.68(1)	2.67(2)	2.65(9)	2.61(12)
Fe–S (Å) mean	2.33(2)	2.33(2)	2.33	4 at 2.52 2 at 2.77
$V(Fe_4)$ (Å^3)	2.26	2.25	2.17	
$V(S_4)$ (Å^3)	6.14	6.21	6.21	
$V(Fe_4S_4)$ (Å^3)	9.47	9.48	9.23	

[a] Reference 23.

[b] Reference 10.

[c] Reference 8.